Irrigation infrastructure prevalence is associated with amplified agricultural water use efficiency drought sensitivity: evidence from Chile's megadrought

(This paper is a non-peer reviewed preprint submitted to EarthArXiv)

Francisco Zambrano[a,*], Francisco Fernández[b], María Molinos-Senante[c]

[a] *Facultad de Medicina Veterinaría y Agronomía, Universidad de Las Américas, Chile,*

[b] *Facultad de Economía, Negocios y Gobierno, Universidad San Sebastián, Santiago, Chile,*

[c] *Institute of Sustainable Processes, Universidad de Valladolid, Valladolid, Spain, 47011*

Abstract

Agricultural water use efficiency (WUE) is widely expected to improve with advances in irrigation technology, yet its response to prolonged drought remains poorly understood at regional scales. We analyzed spatiotemporal patterns of WUE across 127 Chilean agricultural sub-watersheds from 2001 to 2020, a period marked by an unprecedented megadrought. WUE declined broadly across arid and semi-arid regions, driven primarily by precipitation deficits and intensified atmospheric evaporative demand, with the largest declines concentrated in the Mediterranean-climate zone where irrigated agriculture is most prevalent.

Crop system composition is associated with WUE drought sensitivity through two contrasting patterns, each constrained by a different form of confounding. Annual-crop prevalence is negatively associated with drought sensitivity and is robust to latitude control; the causal direction, whether annual-crop presence structurally buffers drought sensitivity, or whether drought stress itself reduces annual cultivation in sensitive watersheds, cannot be established from cross-sectional data alone. Irrigation infrastructure prevalence is positively associated with stronger WUE-drought coupling in the full sample (SEM $\beta = +0.422$, $\rho < 0.001$), consistent with demand-hardening theory, but attenuates substantially when latitude is explicitly controlled ($\beta = +0.109$, $\rho = 0.327$) and cannot be statistically isolated from the latitudinal aridity gradient. Both patterns are hypotheses consistent with the data rather than definitively isolated causal effects.

These findings suggest that hydroclimatic pressures associated with sustained aridification can outweigh gains from technological adaptation, and that agricultural systems with limited crop-type flexibility may remain structurally exposed to drought-coupled supply failure, with implications for water governance in dryland regions globally.

Keywords: water use efficiency, megadrought, aridification, SPEI, Chile, NPP/ET, crop composition

1. Introduction

Global agriculture consumes approximately 70% of freshwater withdrawals (Hoekstra and Mekonnen, 2012), yet whether irrigation infrastructure buffers or amplifies agricultural water use efficiency (WUE) sensitivity under prolonged drought remains poorly understood. The widely held assumption that irrigation protects crop production from meteorological variability has been challenged on two fronts. The irrigation efficiency paradox shows that technical efficiency gains can paradoxically increase aggregate water consumption by enabling crop intensification (Grafton et al., 2018; Ward and Pulido-Velázquez, 2008). Demand-hardening dynamics predict that structural commitment to irrigation infrastructure creates inelastic water demand that amplifies drought vulnerability when supply fails, while annual crop flexibility provides only partial adjustment capacity (Grafton et al., 2018). Whether these mechanisms operate at the watershed scale under a multi-year megadrought, and specifically how they interact with the WUE signal, has not been systematically established. WUE, defined as net primary productivity per unit of evapotranspiration, integrates the simultaneous effects of aridification on vegetation productivity and water consumption, providing a systems-level indicator of how efficiently agricultural land converts available water into biomass (Hoover et al., 2023; Ito and Inatomi, 2012). As aridification intensifies across dryland and Mediterranean-climate regions (Gebrechorkos et al., 2025; Zambrano et al., 2025), whether managed irrigation systems buffer or transmit hydroclimatic stress is a critical question for adaptive water governance (FAO y ONU Agua, 2025; Howden et al., 2007; Wallace, 2000).

Chile provides a compelling natural experiment. Since approximately 2010, central Chile has experienced a persistent megadrought reducing annual precipitation by 20–40% relative to the twentieth-century mean and depleting streamflows across the country's most productive agricultural zones (Boisier et al., 2018; Garreaud et al., 2017, 2020). Atmospheric evaporative demand has also intensified as warming elevated vapor pressure deficit, compounding water stress beyond what precipitation-only indices capture (Li et al., 2023; Zambrano et al., 2025). Chile's central valleys draw primarily on Andean snowmelt-fed rivers whose supply co-varies with regional drought anomalies. When drought reduces both precipitation and snowpack simultaneously, irrigated systems may face amplified rather than reduced hydroclimatic exposure (Garreaud

*Corresponding author
Email addresses: fzambrano@udla.cl (Francisco Zambrano), francisco.fernandez@uss.cl (Francisco Fernández), maria.molinos@uva.es (María Molinos-Senante)

et al., 2020). Agricultural crop composition likely modulates this response: perennial fruit crops dominating export agriculture maintain year-round root systems and may sustain higher net primary production (NPP) under deficit conditions, whereas annuals experience sharper productivity collapses once critical thresholds are breached (Chakraborti et al., 2023; Davis et al., 2017).

This paper addresses the following primary question: Does irrigation infrastructure prevalence buffer or amplify agricultural WUE sensitivity to aridification during the Central Chile Megadrought, and does the pattern align with demand-hardening dynamics? Secondary questions ask: (i) Which aridification signal, SPEI (Standardized Precipitation-Evapotranspiration Index), SPI (Standardized Precipitation Index), or EDDI (Evaporative Demand Drought Index), most strongly predicts WUE variability? (ii) Do NPP or ET (actual evapotranspiration) trends show stronger covariance with WUE change? (iii) Are WUE responses spatially clustered in ways that concentrate agricultural vulnerability? We treat aridification as a multi-process phenomenon using three complementary drought indices: SPEI (Vicente-Serrano et al., 2010), which captures the hydroclimatic balance; SPI (Mckee et al., 1993), which isolates precipitation deficits; and EDDI (Hobbins et al., 2016; McEvoy et al., 2016), which characterizes atmospheric evaporative demand independently of precipitation (AghaKouchak et al., 2015; Zambrano et al., 2025). A paired-census quasi-experimental design applies the same crop-composition regression to both the 2007 (pre-drought) and 2021 (post-drought) agricultural censuses within a spatial error model framework, testing whether elevated WUE sensitivity reflects structural properties predating the megadrought or adaptive responses to it.

2. Data and Methods

2.1. Study area

Continental Chile (approximately 17°S to 56°S) spans extreme latitudinal climate gradients, from the hyperarid Atacama in the north to the Mediterranean zone (32°S–38°S) concentrating the majority of irrigated agriculture, viticulture, and fruit export production, and a humid-temperate zone supporting rainfed cereals and forages south of 38°S (Figure 1). The megadrought most severely affected the 30°S–42°S band, where precipitation deficits of 25–45% relative to the twentieth-century mean have persisted since 2010 (Boisier et al., 2018; Garreaud et al., 2020). The study uses watershed-level spatial units based on Chilean National Water Authority (DGA) hydrological boundaries, which align with the country's water allocation governance framework (Rivera et al., 2016). Chile's 1981 Water Code established a privatized, market-based water governance system in which water rights are tradeable property and drought allocation is governed primarily

by seniority and market exchange rather than state emergency intervention (Malagueño and D'Odorico, 2024).

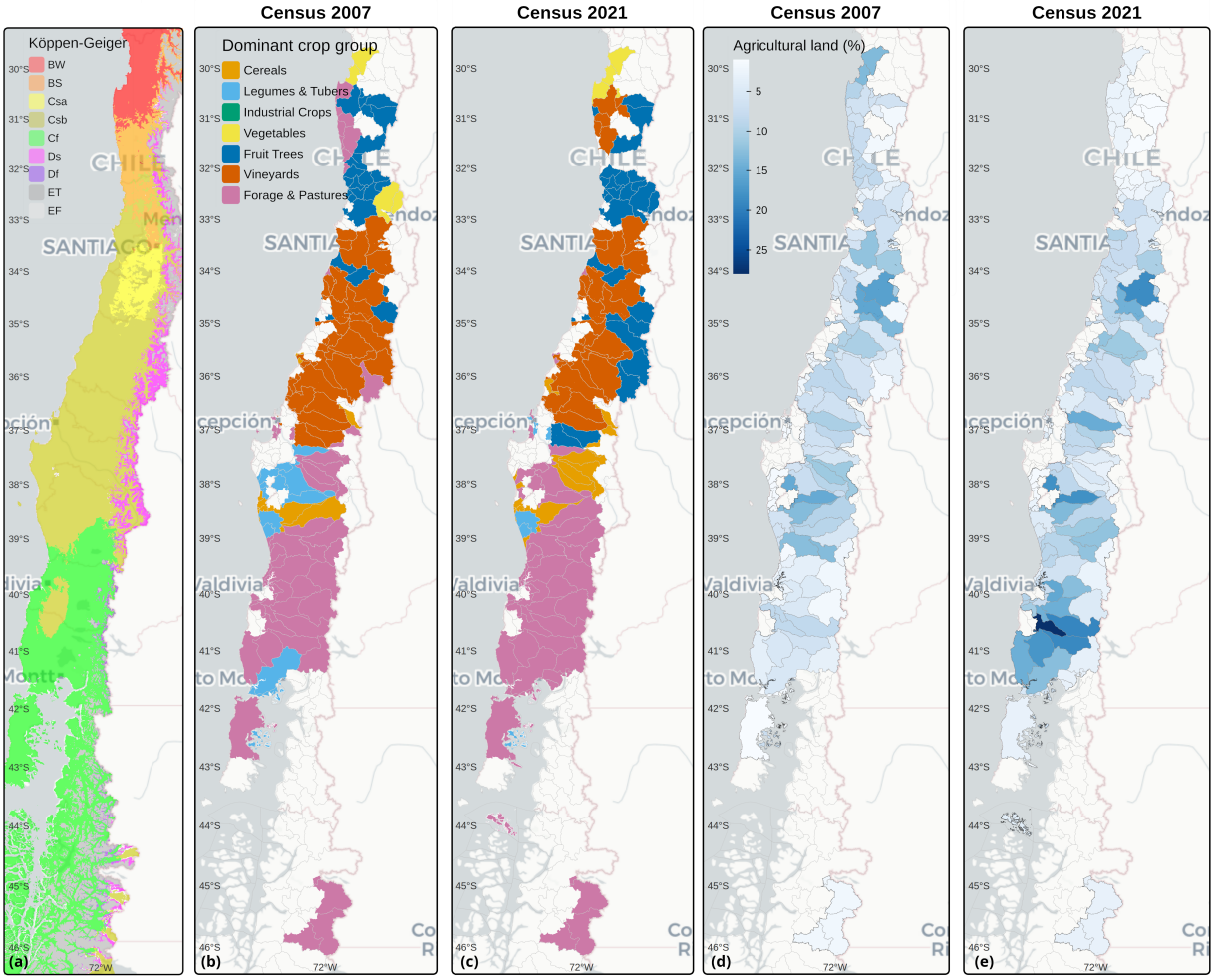

Figure 1: Study area and agricultural context across central Chile. (a) Köppen-Geiger climate classification (2-letter classes) across the study domain, spanning arid (BW) and semi-arid (BS) zones in the north, the warm- and hot-summer Mediterranean centre (Csa, Csb), and the humid-temperate south (Cf). (b-c) dominant agricultural crop group per sub-watershed, derived from the VII (2007) and VIII (2020-2021) Chilean Agricultural and Forestry Censuses. (d-e) agricultural land as a percentage of total sub-watershed area for the same two census years. Sub-watershed boundaries (DGA) are outlined in grey.

2.2. WUE data

Annual cropland WUE ($g\,C\,kg^{-1}\,H_2O\,yr^{-1}$), defined as $WUE = NPP/ET$, was obtained from the global cropland WUE dataset of Jiang et al. (2025), providing 1-km annual rasters for 2001–2020. NPP was estimated using an Evaporative Fraction Light-Use Efficiency (EF-LUE) model driven by ERA5-Land reanalysis, GLASS fAPAR and LAI, and ESA CCI-LC land cover, calibrated against FLUXNET2015 flux towers across multiple climate zones. ET was obtained from the ETMonitor product (Hu and Jia,

2015), validated against flux towers ($r > 0.75$). WUE rasters were cropped to Chile's extent and annual mean WUE was extracted per sub-watershed by spatial averaging. The 20-year series (2001–2020) spans a pre-megadrought reference period (2001–2009) and the megadrought period (2010–2020).

2.3. Drought drivers and WUE mechanistic components

2.3.1. Aridification drivers

Three complementary drought indices characterize distinct aridification dimensions (AghaKouchak et al., 2015; Zambrano et al., 2025). SPEI (primary driver) captures the hydroclimatic balance incorporating both precipitation and atmospheric evaporative demand (Vicente-Serrano et al., 2010). It was computed from CHIRPS (Climate Hazards Group InfraRed Precipitation with Station data) monthly precipitation (Funk et al., 2015) and FAO-56 Penman-Monteith reference evapotranspiration derived from CHIRTS-daily temperature data (Climate Hazards Center Infrared Temperature with Stations, (Funk et al., 2019)), then aggregated to a monthly basis. SPI isolates precipitation deficits from the same CHIRPS series (Mckee et al., 1993). EDDI characterizes anomalies in atmospheric evaporative demand independently of precipitation (Hobbins et al., 2016; McEvoy et al., 2016), computed from CHIRTS-based derived reference evapotranspiration. We used the EDDI sign convention to indicate that positive values represent below-normal evaporative demand, while negative values signify above-normal demand, thereby aligning EDDI with the polarity of SPEI and SPI. Each index was computed at 12, 24, and 36-month accumulation scales. The three indices were standardized via the empirical probability-weighted normal approximation. The December value for each year was retained as the annual index observation. Per-watershed spatial analyses are reported at the accumulation scale maximizing mean per-watershed explanatory power: SPEI-12, SPI-12, and EDDI-24 (mean per-watershed $R^2 = 0.280$, 0.264, and 0.143, respectively).

All three drought indices are derived from CHIRPS precipitation and CHIRTS temperature data, which are observation-based satellite-gauge merged products independent of the ERA5-Land reanalysis used by the EF-LUE model. SPI, which relies on CHIRPS precipitation alone with no temperature or VPD component, shows practically equivalent cross-sectional explanatory power to SPEI at the 36-month scale (mean $R^2 = 0.229$ vs. 0.240; TOST (Two One-Sided Tests) within ± 0.05 R^2 margin: $p < 0.001$, 90% CI $[-0.004, +0.003]$). If shared forcing inflated the WUE–SPEI association, SPI should be substantially weaker. This equivalence provides strong grounds for treating the WUE–drought associations as reflecting genuine biophysical responses. The central inferential result, the crop composition spatial error model, uses relative cross-watershed sensitivity rankings unaffected by any spatially uniform inflation.

2.3.2. WUE mechanistic components

We used the NPP (MOD17A3HGF, MODIS Terra, 500 m, Collection 6.1), which was z-score standardized within 2001-2020 (zNPP), and SETI-12 (Standardized Evapotranspiration Index, 12-month scale; derived from MOD16A2GF actual evapotranspiration (Running et al., 2021)). These are used exclusively as descriptive spatial context variables for the trend comparison in Section 3.1. The primary CASEarth WUE dataset does not distribute its internal NPP (EF-LUE model) and ET (ETMonitor) component layers separately, making algebraic decomposition infeasible. Because MOD17 and MOD16 have different sensitivities and error structures from the EF-LUE and ETMonitor models, zNPP and SETI-12 are not used for formal component attribution of WUE variance, and no cross-product comparison of their relative sensitivities is presented.

2.4. Agricultural census data

Crop composition data were obtained from the VII Census (2007, pre-drought baseline) (INE, 2007) and the VIII Census (2020–2021, endpoint) (INE, 2021), both reporting cultivated area by crop category and management type at commune level. Commune-level data were spatially aggregated to watershed level using area-weighted means. Three functional aggregates were computed for use as regression predictors: *pct_perennials* (fruit trees + vineyards), *pct_annuals* (cereals + vegetables + legumes + industrial crops), and *pct_forage* (forage/pasture; reference category). The variable *pct_irrigated* measures the census-reported proportion of agricultural land classified as irrigated, reflecting irrigation infrastructure and historical water rights, not the volume of water actually delivered in any given year. Sub-watersheds with high *pct_irrigated* have more irrigation-dependent cropping systems and greater structural exposure to supply disruptions. Dominant crop type per watershed was assigned using a 40% area threshold.

The 2021 census irrigated area variable is derived entirely from directly reported data and underpins the primary spatial error model results. The 2007 irrigated area variable required partial imputation because the main 2007 census publication reports only total crop area by category, without a riego/secano split, for six of ten crop categories (fruit trees, vegetables, flowers, forages, seed crops, nurseries). For the remaining six categories, a commune-level residual ratio was computed as follows: (i) total communal irrigated area in 2007; (ii) the directly known irrigated area (cereals + industrial crops + vineyards) was subtracted; (iii) the residual irrigated area was divided by the total area in the six imputed categories to yield a commune-specific ratio; and (iv) this ratio was applied uniformly to each of the six imputed categories for that commune. This methodology uses only 2007 census data, no post-drought data, 2021 values, or time-invariant spatial proxies enter the imputation. National totals are preserved to within 5% for all categories. The imputation applies

a single commune-level ratio across the six categories rather than category-specific ratios. Because crop categories likely have very different true irrigation intensities (fruit trees may be nearly fully irrigated while forages may be largely rainfed), this uniform ratio fundamentally distorts the cross-sectional variance structure of the 2007 pct_irrigated variable. Sub-watersheds that would show strong cross-sectional differentiation in a truly measured predictor are conflated by the uniform ratio. The 2007 irrigated area variable therefore does not represent the same quantity as the directly reported 2021 variable, and the apparent similarity in regression coefficients (2007 SEM $\beta = +0.467$ vs. 2021 $\beta = +0.422$) cannot serve as reliable evidence for structural stability of the irrigation finding. Furthermore, in a multiple regression framework, severe measurement error in one predictor biases the coefficient estimates of other correlated predictors. Given the acknowledged spatial collinearity between pct_irrigated and pct_annuals, the distortion in the 2007 pct_irrigated variable likely spills over to affect the 2007 annual-crops coefficient, rendering it unreliable as a comparator regardless of whether the crop area totals themselves are directly reported. The entire 2007 model comparison should therefore be treated as uninformative for all three predictors. The imputation code is available at the project repository.

2.5. Statistical analyses

2.5.1. Trend and change-point analyses

Mann-Kendall trend tests and Sen's slope estimates (with prewhitening) were computed per watershed for WUE, zNPP, SETI-12, and EDDI-12 (2001-2020). The Pettitt test (Pettitt, 1979) was applied to each WUE series to detect the most probable year of mean-level shift. Benjamini-Hochberg (BH) false-discovery-rate (FDR) correction was applied across 131 simultaneous tests. Watersheds were classified by significance (rho < 0.05) and proximity to megadrought onset (break years within ± 2 years of 2010). A permutation null model (B = 1000 iterations per watershed, seed = 2026) tested whether the observed break-year concentration near 2010 is distinguishable from a SPEI-step-change tracking null. Within-watershed residuals from a SPEI-12 OLS (ordinary least squares) regression were resampled with replacement and the Pettitt test was re-run on each reconstructed null series. Observed and null break-year distributions were compared using a two-sample Kolmogorov-Smirnov (KS) test. Mean WUE was compared between the pre-megadrought (2001-2009) and megadrought (2010-2020) periods using Wilcoxon signed-rank tests, stratified by Köppen climate class.

2.5.2. WUE-aridification relationships

Spearman correlations and OLS sensitivity slopes ($\Delta WUE/\Delta Index$) were computed per watershed across the 20-year series. Per-watershed maps are treated as descriptive summaries given strong spatial autocorrela-

tion (Moran's I = 0.509-0.683); confirmatory inference rests on the spatial error models and FDR-corrected Pettitt analysis. Moran's I and Getis-Ord Gi* local statistics identified spatial clustering and hotspots of WUE trend slope using queen contiguity weights. A two-way fixed-effects (TWFE) panel regression estimated:

$$WUE_{it} = \beta \cdot Index_{it} + \mu_i + \tau_t + \varepsilon_{it} \tag{1}$$

where μ_i and τ_t are watershed and year fixed effects. Standard errors are Driscoll-Kraay (DK; Driscoll and Kraay (1998); bandwidth = 2), consistent for both serial correlation and cross-sectional spatial dependence. DK SEs inflate 3–4× relative to conventional HC1 (Heteroskedasticity-Consistent) clustered SEs, reflecting the strong spatial common component (full comparison in Supplementary Table S-11).

2.5.3. Crop composition and WUE sensitivity

The per-watershed OLS slope of WUE regressed on SPEI-12 was used as the outcome in a multiple regression:

$$Sensitivity_i = \beta_0 + \beta_1 \cdot pct\_perennials_i + \beta_2 \cdot pct\_annuals_i + \beta_3 \cdot pct\_irrigated_i + \varepsilon_i \tag{2}$$

with forage/pasture as the reference category. Variance inflation factors confirmed the absence of harmful multicollinearity (all VIF < 5). Where OLS residuals were spatially autocorrelated (Moran's I, $p < 0.05$), a spatial error model (SEM) was fitted as the primary inferential model.

The TWFE panel introduced in Section 2.5.2 is estimated over the same 127 sub-watersheds; its non-significant Driscoll-Kraay results (Section 3.5) may appear to undermine the two-stage SEM, but the two approaches ask fundamentally different questions and address distinct statistical quantities. The panel estimates the *pooled mean* $\bar{\beta} = E[\beta_i]$: Driscoll-Kraay SEs make this uncertain because contemporaneous cross-sectional dependence reduces the effective independent information available to pin down the common temporal slope. The SEM, by contrast, uses the *cross-sectional dispersion* of per-watershed slopes β_i, testing whether irrigation-dense watersheds show systematically larger β_i than rainfed watersheds. These are separable quantities: $E[\beta_i]$ can be uncertain while $\mathrm{Var}(\beta_i)$ is real and structured. A concern that per-watershed OLS slopes are "spurious" because they capture a common year-effect conflates these two

estimands. When a common drought signal simultaneously depresses SPEI across all watersheds, β_i measures how strongly each watershed's WUE co-moves with that signal, a valid and interpretable measure of local coupling strength. An irrigation-dense watershed with $\beta_i = 0.8$ genuinely shows stronger drought coupling than a rainfed watershed with $\beta_i = 0.1$, regardless of whether the pooled mean is identifiable. Moran's I = 0.514 ($p < 0.001$) on the observed β_i values confirms this cross-sectional variation is spatially organized rather than noise.

The identical three-predictor specification was applied to the 2007 pre-drought census data across the same 127 sub-watersheds. However, as detailed in Section 2.4, this comparison is unreliable for all three predictors: the 2007 pct_irrigated is 66.6% imputed with a fundamentally distorted cross-sectional variance structure, and measurement error in this correlated predictor spills over to bias the 2007 annual-crops and perennial-crops coefficients in a multiple regression framework. The 2007 model results are therefore reported for transparency but cannot support or refute structural stability for any predictor. Robustness was verified through: (i) restriction to within-Csb warm-summer Mediterranean sub-watersheds (n = 67); (ii) a synchronized-time bootstrap (B = 1000) propagating stage-1 estimation uncertainty while preserving cross-sectional spatial covariance (Supplementary Table S-10); (iii) a barren-exclusion dynamic land-cover filter excluding MODIS-confirmed non-vegetated pixels (Supplementary Table S-7); (iv) a parallel SEM using the Standardized Snow Water Equivalent Index (SWEI) from ERA5-Land as the drought predictor (Supplementary Table S-6); and (v) addition of sub-watershed centroid latitude as a direct covariate to test whether the irrigation association persists after explicit control for the latitudinal aridity gradient (Supplementary Table S-14).

2.6. Software

All statistical analyses and spatial processing were conducted in R (v4.5.2; R Core Team (2025)). Raster operations and spatial aggregation used `terra` (v1.8.54; Hijmans (2025)). Vector geometries and spatial joins used `sf` (v1.0.23; Pebesma (2018), Pebesma and Bivand (2023)). Spatiotemporal array operations used `stars` (v0.6.8; Pebesma and Bivand (2023)). Mann-Kendall trend tests and Sen's slope estimation with prewhitening used `modifiedmk` (v1.6; Patakamuri and O'Brien (2021)) and `trend` (v1.1.6; Pohlert (2023)). Spatial autocorrelation (Moran's I, Getis-Ord Gi*) and spatial weight matrices used `spdep` (v1.4.1; Bivand and Wong (2018)). Spatial Error Model was made using `{spatialreg}` (Bivand et al., 2021). Panel regression with fixed effects used `plm` (Croissant and Millo, 2008); Driscoll-Kraay standard errors via `plm::vcovSCC` (Driscoll and Kraay, 1998); HC1 clustered SEs via `plm::vcovHC` with `lmtest::coeftest`. Variance inflation

factors used `car` (v3.1.3; Fox and Weisberg (2019)). General-purpose data manipulation and reshaping used `tidyverse` (v2.0.0; Wickham et al. (2019)), including `dplyr`, `tidyr`, `readr`, `stringr`, `purrr`, and `lubridate`. Thematic maps used `tmap` (v4.2; Tennekes (2018)). Statistical graphics used `ggplot2` (v3.5.2; Wickham (2016)). Multi-panel figure layout used `patchwork` (v1.3.1; Pedersen (2025)).

3. Results

3.1. Long-term WUE trends

Trend analysis across 127 Chilean agricultural sub-watersheds revealed predominantly negative WUE trends across the Mediterranean-climate zone (approximately 30°S–35°S), consistent with megadrought onset and intensification (Figure 2).

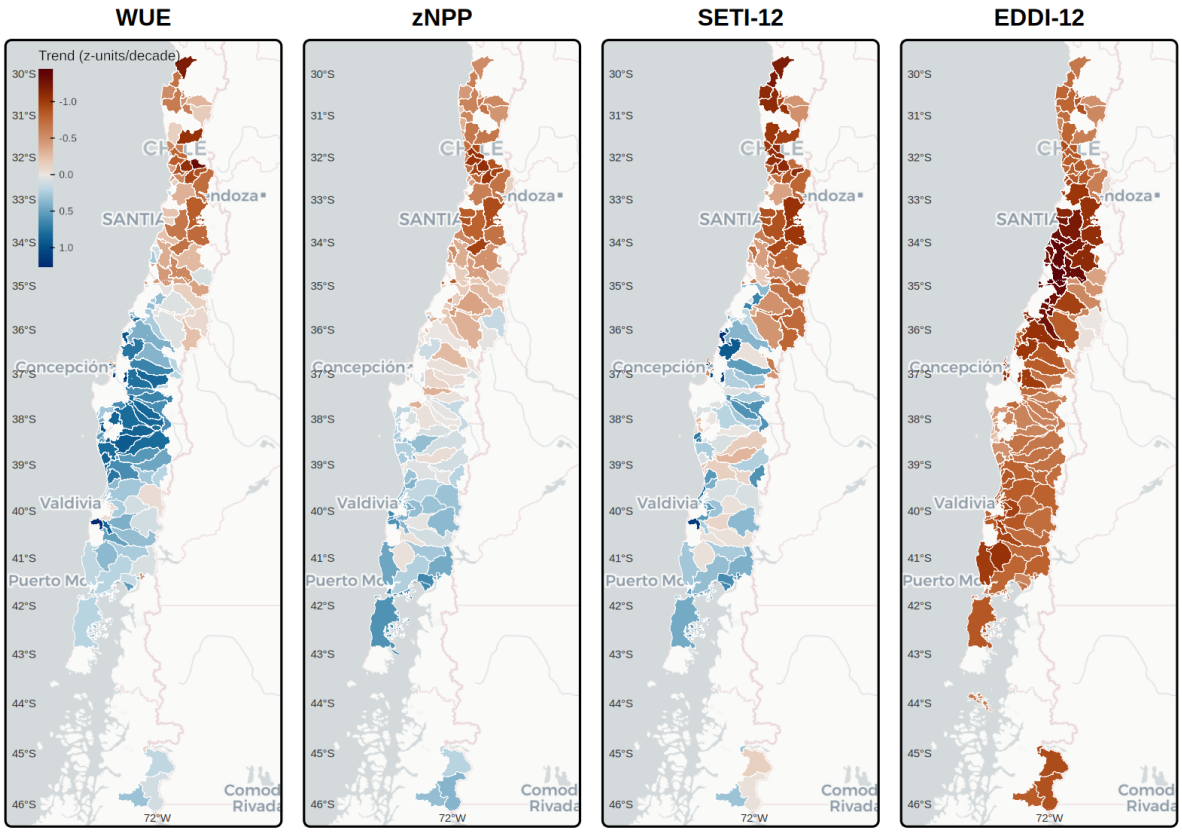

Figure 2: Spatial distribution of long-term trends in WUE, zNPP (NPP anomaly), SETI-12 (12-month ET anomaly), and EDDI-12 (12-month atmospheric evaporative demand) across Chilean watersheds (2001-2020). Trend magnitudes are expressed as z-score standardized Sen's slope estimates.

zNPP (MOD17A3HGF) and SETI-12 (MOD16A2GF) are independent proxy products that do not decompose

the CASEarth WUE directly; the following patterns are descriptive spatial co-variation, not formal component attribution. zNPP trends exhibit strong spatial covariance with WUE, with negative anomalies concentrated in the same central Mediterranean watersheds where WUE declines are most pronounced. SETI-12 trends are more spatially complex: sub-watersheds where ET declined less steeply than NPP tend to show WUE decline, while those where ET reduction exceeded NPP reduction tend toward stable or improving WUE. Declining WUE is spatially co-located with negative NPP anomalies, while ET responses are heterogeneous and modulated by irrigation access and crop type. Whether NPP suppression is a more proximate correlate of WUE decline than ET cannot be formally established from these proxy data, as the independent products may differ in sensitivity and error structure from the EF-LUE and ETMonitor components underlying the CASEarth WUE (Fifth limitation, Section 4.5).

3.2. WUE change-point analysis

The Pettitt test detected FDR-significant mean-level change points in 22 of 131 sub-watersheds (adjusted p range: 0.019–0.047), all dated 2009–2012. These FDR-significant breaks are geographically concentrated in the central Mediterranean zone, the core of the megadrought's hydroclimatic footprint, while the arid north and wet south show no FDR-significant breaks aligned with 2010 (Boisier et al., 2018; Garreaud et al., 2020). This geographic patterning is the primary informational content of the analysis, it identifies which sub-watersheds' WUE dynamics were most tightly coupled to megadrought forcing (Figure 3 a). Break years were not significantly spatially clustered (Moran's I = 0.018, p = 0.345), indicating the temporal concentration near 2010 reflects common large-scale forcing rather than spatial propagation. The permutation null model showed 72.1% of null Pettitt tests also had break years within ±2 years of 2010 (observed: 84.1%); the Kolmogorov-Smirnov test detected no significant difference (D = 0.153, p = 0.255), a failure to reject the null that does not permit an affirmative equivalence claim.

3.3. WUE before and after the megadrought

Mapping $\Delta WUE = WUE_{post} - WUE_{pre}$ per watershed revealed pronounced spatial heterogeneity (Figure 3 b). Arid and semi-arid sub-watersheds showed predominantly negative ΔWUE, while irrigated Mediterranean and humid-temperate sub-watersheds showed positive ΔWUE. The aggregate Wilcoxon signed-rank test was positive and significant (p = 0.007), but this reflects the numeric dominance of irrigated Mediterranean sub-watersheds, not widespread drought resilience. Köppen-stratified analyses resolve the heterogeneity (Supplementary Table S-2). BW (hot desert; n = 8) showed significant declines (Hodges-Lehmann estimate = −0.535, 95% CI: −0.862 to −0.335; p = 0.008), as did BS (semi-arid steppe; n = 14; HL = −0.643, $p < 0.001$).

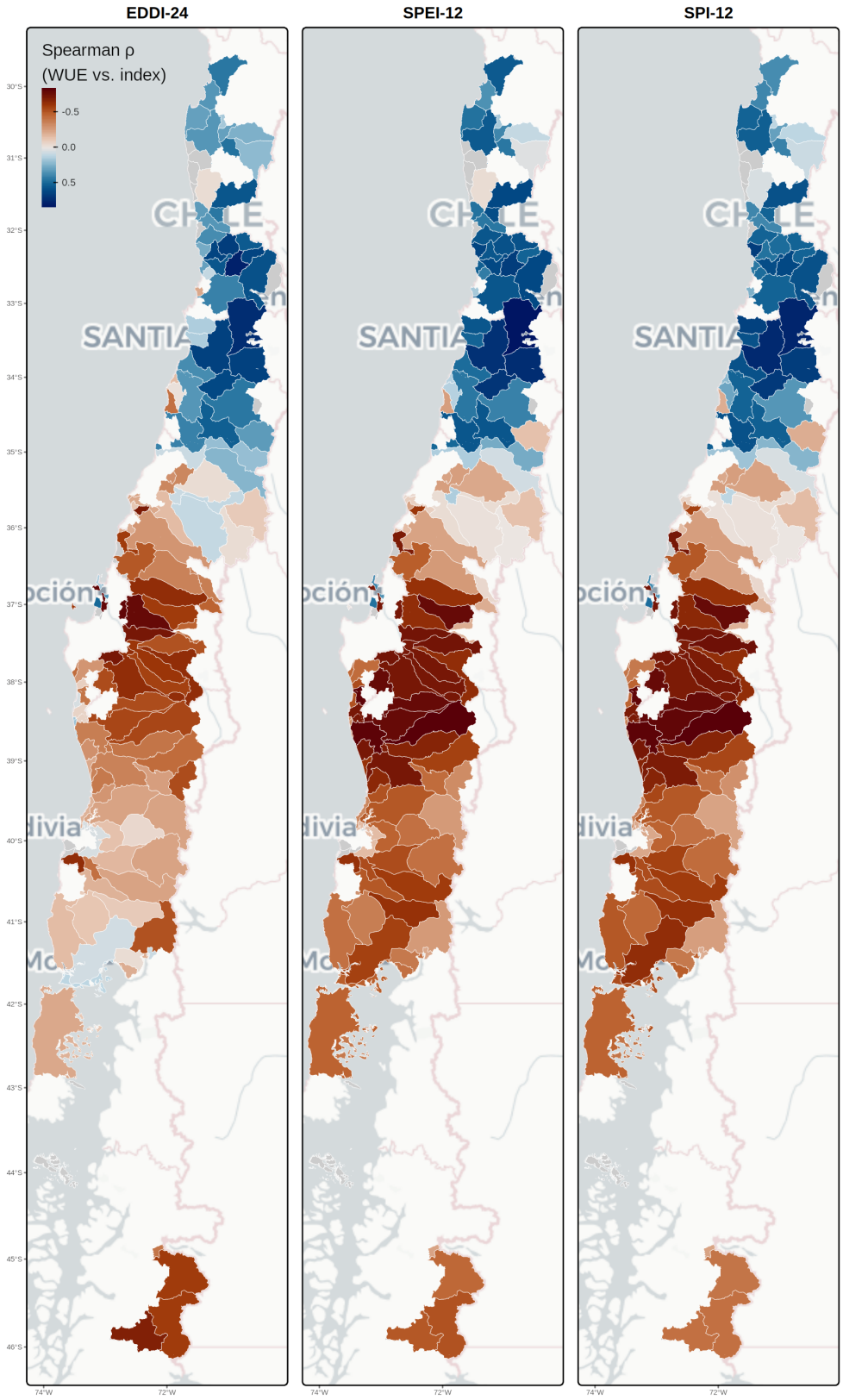

Figure 3: (a) Spatial distribution of Pettitt change-point years in annual WUE per watershed (significant at $p < 0.05$). Watersheds with change-point years within ±2 years of 2010 are highlighted with bold borders; the geographic concentration of FDR-significant breaks in the central Mediterranean zone identifies which sub-watersheds' WUE most tightly tracked the SPEI megadrought step-change (see Section 3.2). Non-significant change points are shown in grey. (b) Spatial map of WUE change between the megadrought period (2010–2020) and the pre-megadrought period (2001–2009) ($\Delta WUE = WUE_{post} - WUE_{pre}$) per watershed. Positive values (blue) indicate net WUE increase; negative values (red) indicate WUE decline. Köppen climate zone boundaries (dashed lines) are overlaid. (c) Violin-boxplot distributions of annual WUE for the pre-megadrought (blue, 2001–2009) and megadrought (red, 2010–2020) periods, stratified by Köppen climate class. Each panel corresponds to one climate class; y-axes are free-scaled.

Csb (warm-summer Mediterranean; n = 71) and Cf (humid subtropical; n = 26) exhibited significant WUE increases (HL = +0.374, $p < 0.001$ and HL = +0.367, $p < 0.001$, respectively). Violin-boxplot distributions stratified by Köppen class (Figure 3 c) confirm this divergence.

3.4. WUE responses to aridification signals

Spearman correlation analysis at the per-family optimal scales (SPEI-12, SPI-12, EDDI-24) revealed positive associations between annual WUE and drought indices across most Chilean watersheds (Figure 4), with wetter years generally associated with higher WUE.

At the 36-month scale, SPEI and SPI showed practically equivalent associations with WUE (mean R^2 = 0.240 and 0.229; TOST within ±0.05 margin: $p < 0.001$, 90% CI [−0.004, +0.003]), both significantly outperforming EDDI-36 (mean R^2 = 0.140; $p < 0.001$; Supplementary Figure S-2). The precipitation component dominates the spatial gradient in WUE variability at multi-year accumulation scales.

3.5. Panel regression: temporal WUE-drought relationships

Under Driscoll-Kraay standard errors, no panel coefficient reaches conventional significance at any index or accumulation scale. SPEI-12 ($\beta = -0.112$, DK $\rho = 0.273$), SPI-12 ($\beta = -0.170$, DK $\rho = 0.053$), and Mediterranean-restricted SPEI-24 ($\beta = +0.193$, DK $\rho = 0.458$) and SPI-24 ($\beta = +0.141$, DK $\rho = 0.579$) are all non-significant (Supplementary Table S-11). The negative signs at the 12-month scale arise from humid-temperate Cf sub-watersheds (n = 26), where rainfed annual systems transiently raise WUE under mild moisture stress (Yu et al., 2020). The substantive interpretation is that WUE-drought co-variation in the temporal panel is largely a spatially common signal. The same calendar years are simultaneously wet or dry across all Mediterranean watersheds, leaving insufficient independent within-unit variation to support inference once cross-sectional dependence is properly accounted for. The drought index's physical role in determining WUE sensitivity is established through the cross-sectional sensitivity slopes (Section 3.6, Section 3.7) and the DGA streamflow validation (Section 4.3), not through the panel temporal analysis. Full HC1 vs. DK comparison is in Supplementary Table S-11.

3.6. Spatial distribution and clustering of WUE sensitivity

The WUE-SPEI-12 sensitivity map (Figure 5 a) shows the OLS slope per watershed. Sensitivity broadly follows the latitudinal aridity gradient, with central Mediterranean watersheds exhibiting higher values than humid southern watersheds and locally elevated sensitivity in perennial-dominated irrigated zones (Figure 5 b and c).

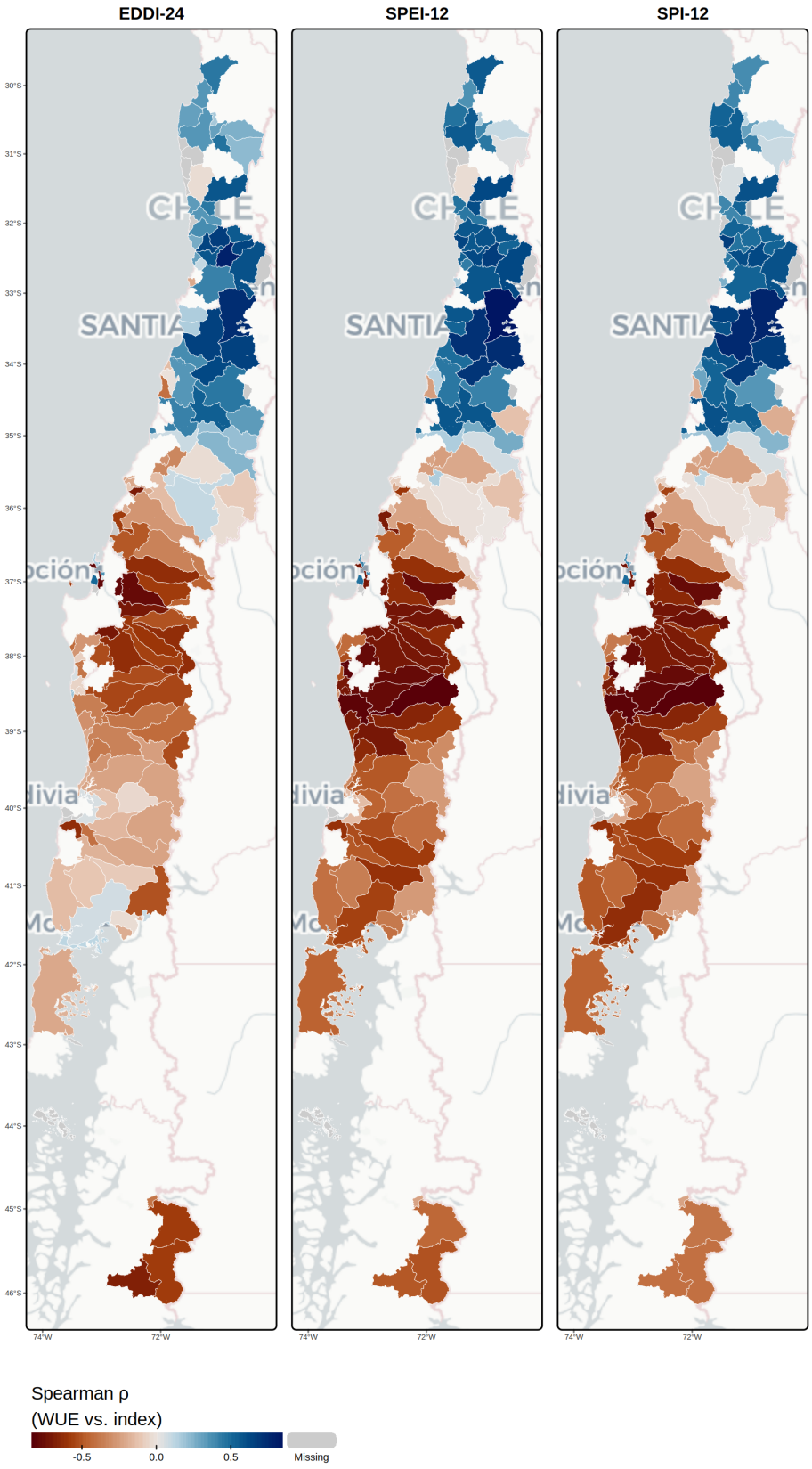

Figure 4: Spatial maps of Spearman (WUE vs. drought index) per watershed, faceted by drought index at the accumulation scales used for the per-watershed spatial analyses (SPEI-12, SPI-12, EDDI-24). Diverging colour scale (blue = positive correlation, red = negative correlation).

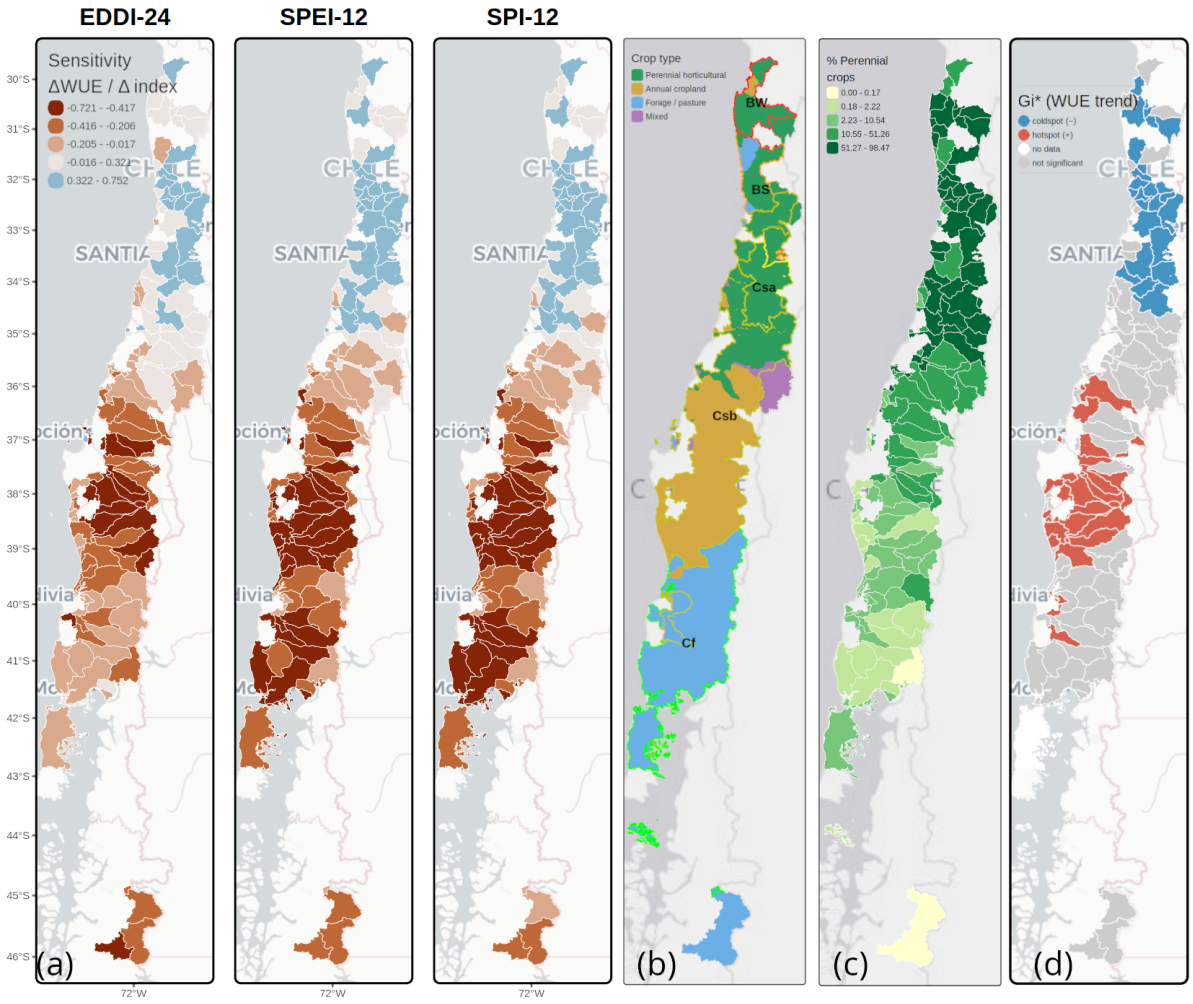

Figure 5: (a) Spatial distribution of WUE-drought sensitivity ($\Delta WUE/\Delta Index$, the OLS slope of the annual WUE ~ index regression per watershed, 2001-2020) for SPEI-12, SPI-12, and EDDI-24. High positive values indicate strong positive WUE response; near-zero or negative values indicate weak or inverted coupling. (b) Choropleth map of dominant crop type per watershed, classified by the agricultural functional group exceeding 40% of total agricultural area (Perennial horticultural, Annual cropland, Forage/pasture, Mixed). (c) Choropleth map of perennial crop share (% of total agricultural area under fruit trees and vineyards) per watershed. (d) Getis-Ord Gi* hotspot analysis of WUE trend slope across Chilean watersheds. Red watersheds are statistically significant hotspots (positive WUE trend clusters; Gi* > 1.96); blue are coldspots (negative WUE trend clusters; Gi* < -1.96); grey are not significant at the 95% level.

Moran's I for WUE trend slope was I = 0.683 ($p < 0.001$) and for WUE-SPEI-12 R^2 was I = 0.509 ($p < 0.001$), confirming strong geographic clustering. Getis-Ord Gi* hotspot analysis identified coherent coldspots in the central Mediterranean zone and localized hotspots in transitional zones (Figure 5 d). Pettitt change-point years were not significantly spatially clustered (I = 0.018, p = 0.345), indicating that the temporal concentration near 2010 reflects common large-scale forcing rather than spatial propagation. Hydroclimate governs when and how strongly WUE shifts over time; crop composition modulates the spatial magnitude of each sub-watershed's drought sensitivity. These two axes are complementary rather than competing.

3.7. Agricultural crop composition and WUE sensitivity

Integration of census-derived crop composition with WUE-SPEI-12 sensitivity estimates (n = 127 sub-watersheds) revealed a clear positive association between irrigated area share and drought sensitivity (Figure 6 a). Watersheds classified as perennial horticultural exhibited the highest median WUE-SPEI-12 sensitivity, forage/pasture watersheds showed the lowest, and annual cropland watersheds showed intermediate sensitivity (Figure 7 a). Because perennial crop distribution, aridity, and WUE sensitivity all co-vary with latitude (Figure 6 c), this pooled perennial association may partly reflect the underlying climate gradient rather than an isolated crop-system effect (Section 4.5).

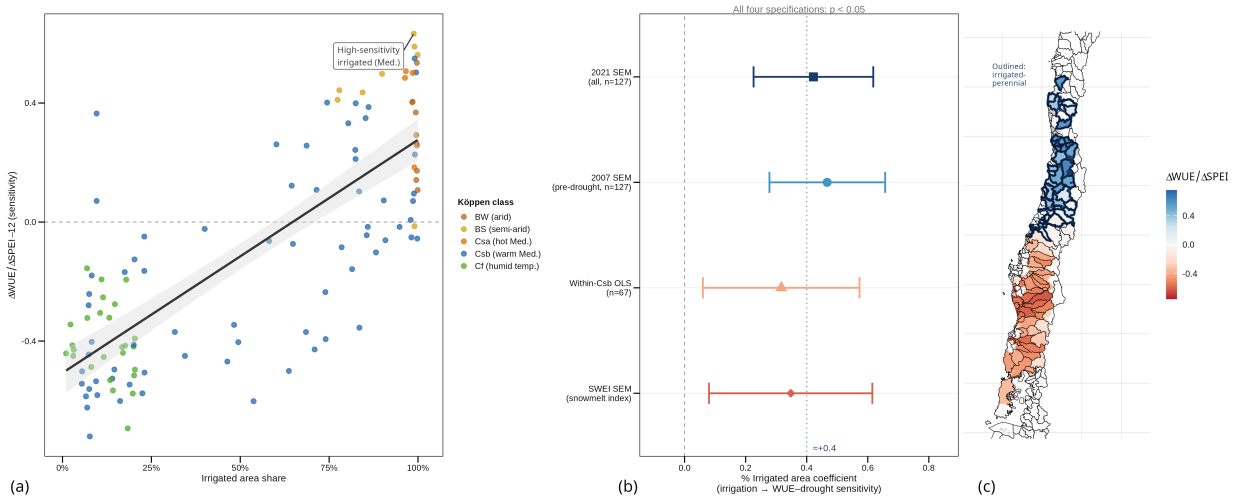

Figure 6: (a) Scatter plot of WUE-SPEI-12 sensitivity versus irrigated area share per sub-watershed (n = 127), coloured by Köppen climate class, with a pooled OLS regression line (±95% CI). Points in the upper-right cluster (high irrigation, high sensitivity) correspond to Mediterranean irrigated-perennial systems; points in the lower-left correspond to rainfed or annual-crop dominated systems. (b) Forest plot of the irrigated area share regression coefficient (±95% CI) across four independent model specifications: 2021 full-sample SEM, 2007 pre-drought SEM, within-Csb (warm-summer Mediterranean) OLS, and SWEI-based SEM using snowmelt index as the drought predictor. All four specifications return a coefficient near +0.32–0.47 (three at $p < 0.05$; within-Csb SEM p = 0.053). The vertical dotted line marks +0.4 for reference. (c) Choropleth of WUE-SPEI-12 sensitivity (OLS slope per watershed, 2001–2020); solid blue borders outline perennial-horticultural-dominant sub-watersheds, which concentrate in the central Mediterranean zone and correspond to the high-sensitivity cluster in panel (a).

The multivariate OLS regression (n = 127 sub-watersheds) returned: irrigated area share as the strongest positive predictor ($\beta = 0.499$, $\rho < 0.001$), indicating that sub-watersheds structurally organised around irrigation infrastructure show stronger WUE-SPEI-12 sensitivity; annual crop share as a significant negative predictor ($\beta = -0.304$, $\rho < 0.001$), indicating buffering relative to the forage/pasture reference; and perennial crop share as a positive but subsequently attenuated predictor ($\beta = 0.359$, $\rho = 0.003$). The irrigated area coefficient captures the association between irrigation infrastructure prevalence and drought coupling, not actual water volumes delivered in drought years.

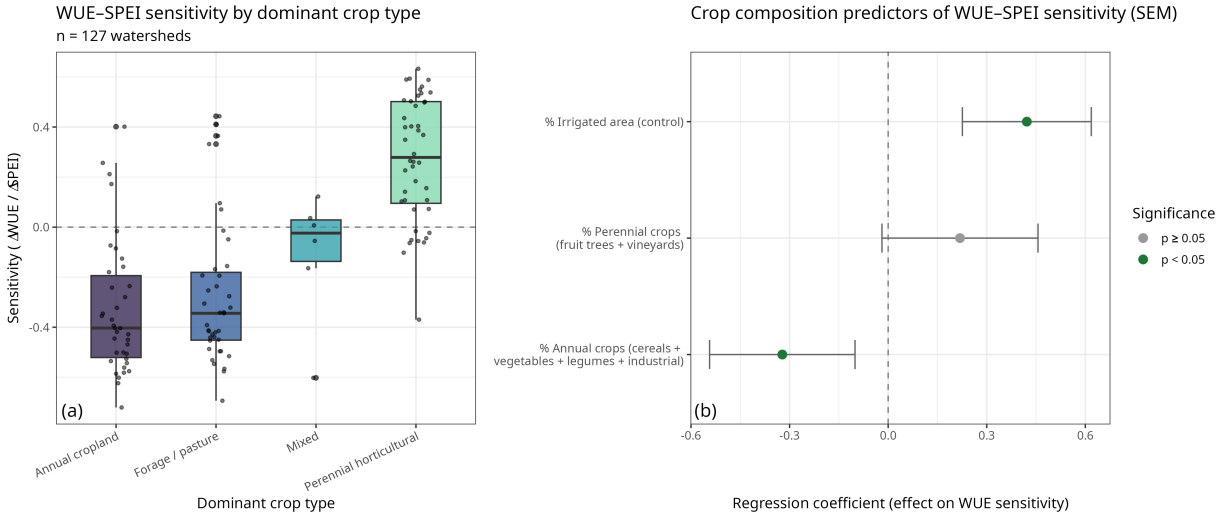

Figure 7: WUE-SPEI-12 sensitivity by dominant crop type (n = 127 sub-watersheds). (a) Boxplot distributions of per-watershed OLS sensitivity slopes stratified by dominant agricultural system: perennial horticultural (fruit trees + vineyards), annual cropland (cereals + vegetables + legumes + industrial crops), and forage/pasture. Perennial-dominated watersheds show the highest median sensitivity; forage/pasture watersheds show the lowest. (b) Full-sample SEM coefficient plot for the three functional-aggregate predictors with 95% confidence intervals; filled symbols indicate $p < 0.05$. Numeric values and within-Csb comparisons are in Table 1.

Moran's I on OLS residuals was I = 0.197 ($\rho = 0.001$), so a spatial error model (SEM; queen-contiguity weights) was fitted as the primary inferential model ($\lambda = 0.468$, $\rho < 0.001$). The SEM attenuated but largely preserved the OLS conclusions: irrigated area share ($\beta = 0.422$, $\rho < 0.001$), annual crop share ($\beta = -0.322$, $\rho = 0.004$), and perennial crop share ($\beta = 0.219$, nominal $\rho = 0.071$; synchronized-time bootstrap $\rho = 0.032$; Figure 7 b). A synchronized-time bootstrap (B = 1000, preserving contemporaneous spatial covariance; Supplementary Table S-10) confirmed all three predictors significant ($\rho = 0.002$-0.032). Bootstrap SEs were 0.74-0.91× the nominal SEM SEs for substantive predictors, and WLS estimates (Supplementary Table S-5) confirm no sign changes under stage-1 uncertainty weighting.

To test whether associations are crop-system properties robust to the latitudinal aridity gradient, the model

was restricted to Csb warm-summer Mediterranean sub-watersheds (n = 67). Results differ strikingly by predictor (Table 1):

Table 1. Comparison of WUE-SPEI-12 sensitivity regressions across model specifications. Full-sample SEM: n = 127 (all climate classes); within-Csb OLS and SEM: n = 67 (warm-summer Mediterranean sub-watersheds only, $\lambda = 0.255$, $\rho = 0.057$). Reference category: forage/pasture. *** $\rho < 0.001$; ** $\rho < 0.01$; * $\rho < 0.05$; † $\rho < 0.10$.

Predictor	Full-sample SEM	Full-sample SEM ρ	Within-Csb OLS β	Within-Csb OLS ρ	Within-Csb SEM β	Within-Csb SEM ρ
% Irrigated area	+0.422	< 0.001 ***	+0.317	0.016 *	+0.264	0.053 †
% Annual crops	−0.322	0.004 **	−0.463	0.004 **	−0.565	0.001 **
% Perennial crops	+0.219	0.071 †	+0.297	0.102	+0.184	0.320

Full results in Supplementary Table S-4.

The irrigated area association survives the Csb restriction in OLS ($\beta = +0.317$, $\rho = 0.016$), attenuating to marginal significance under SEM within Csb ($\beta = +0.264$, $\rho = 0.053$; Figure 6 b). The annual-crops association strengthens within Csb (SEM $\beta = -0.565$, $\rho = 0.001$), confirming this as a genuine crop-system property independent of the latitudinal gradient. Perennial crop share loses significance entirely within Csb (SEM $\beta = +0.184$, $\rho = 0.320$), confirming it is a latitude-aridity co-variation artefact.

The 2007 census comparison is uninformative for all three predictors (Section 2.4). The 2007 pct_irrigated is a synthetic construct with a distorted cross-sectional variance structure, and measurement error in this correlated predictor spills over to bias the 2007 annual-crops and perennial-crops coefficients in the same multiple regression model. The annual-crops association was non-significant in 2007 (SEM $\beta = -0.136$, 95% CI [−0.414, +0.142]) and significant in 2021 ($\beta = -0.322$, 95% CI [−0.543, −0.101]; Supplementary Table S-9), but this difference cannot be attributed to temporal change: the CIs overlap substantially, no formal test of the coefficient difference has been conducted, and the 2007 non-significance may reflect bias from the correlated distorted predictor rather than a truly absent effect. The causal direction of the 2021 negative

association is discussed in Section 4.3.

Natural vegetation contamination within the agricultural mask was non-significant as a control covariate (β = 0.098, ρ = 0.509; Supplementary Figure S-3).

3.8. Accumulation-scale selection and cross-sectional context

Mean within-watershed temporal R^2 at the per-family optimal scales was 0.277 for SPEI-12, 0.264 for SPI-12, and 0.168 for EDDI-24 (Supplementary Table S-12). SPEI-12 and SPI-12 show practically equivalent temporal explanatory power (TOST within ±0.05 margin: $p < 0.001$, 90% CI [+0.007, +0.019]), both substantially exceeding EDDI-24. These values form the basis for accumulation-scale selection and for the stage-1 per-watershed sensitivity slopes.

A cross-sectional variance partition (Supplementary Table S-12 only) is included for transparency: drought indices (SPEI, SPI) are standardized temporal anomalies relative to each watershed's local historical mean and therefore carry little information about the absolute spatial aridity gradient at any single time point. The near-zero unique cross-sectional variance attributable to drought indices is a dimensional artefact of standardization rather than evidence that drought matters less than crop composition for WUE. Drought's role in determining WUE sensitivity is captured through the temporal dimension (within-watershed sensitivity slopes) rather than in single-year cross-sections. Sample sizes for each analytical step are documented in Supplementary Table S-1.

4. Discussion

4.1. The megadrought as a driver of persistent WUE change

That WUE undergoes a mean-level shift concurrent with the megadrought onset is a physically expected consequence of WUE being hydroclimate-driven, not a novel finding. The permutation null model provides no evidence to distinguish the observed break-year concentration from simple SPEI step-change tracking (KS p = 0.255), confirming this expectation. The informative content of the change-point analysis is its spatial specificity: FDR-significant breaks are concentrated in the central Mediterranean zone, identifying which sub-watersheds' WUE dynamics were most tightly coupled to megadrought forcing. The aggregate WUE increase (Wilcoxon p = 0.007) conceals critical spatial heterogeneity. WUE declined in arid northern sub-watersheds while rising in the irrigated Mediterranean zone. This apparent gain does not reflect drought resilience; it coincides with the elevated drought coupling of those same systems documented in Section 4.3.

4.2. Multidimensional aridification: why index choice matters

The practically equivalent performance of SPEI-36 and SPI-36 in cross-sectional analyses (TOST: $p < 0.001$) indicates that the precipitation component dominates the spatial gradient in WUE sensitivity under megadrought conditions. The TWFE panel provides no statistically significant evidence for within-unit temporal WUE-drought coupling at any index or scale once cross-sectional dependence is accounted for through Driscoll-Kraay SEs (Supplementary Table S-11). The substantive interpretation is that WUE-drought co-variation in the temporal panel is largely a spatially common phenomenon. The same calendar years are wet or dry across all Mediterranean watersheds simultaneously, leaving insufficient independent within-unit variation to support inference. Drought's physical role in determining WUE sensitivity is established through the cross-sectional sensitivity slopes and the DGA streamflow validation, not through the panel temporal analysis.

4.3. Irrigation infrastructure and amplified drought sensitivity

In the full-sample SEM without latitude control, census-reported irrigated area share is positively associated with WUE-drought sensitivity ($\beta = +0.422$, $\rho < 0.001$). Sub-watersheds with higher irrigation infrastructure prevalence are more coupled to hydroclimatic variability because their production systems depend on snowmelt-fed surface water supply that co-declines with drought, creating production rigidity when supply fails. The snowmelt co-variation mechanism is supported by three independent lines of evidence: cross-product ρ(CHIRPS SPEI-12, ERA5-Land SWEI) = 0.549 in the most-irrigated quartile; cuenca-level ρ(CHIRPS SPEI-12, DGA annual streamflow) = 0.72-0.83 across the five key irrigation basins (Supplementary Table S-13); and ρ(DGA streamflow, WUE) = 0.38-0.68 in the three northern irrigation basins.

However, adding sub-watershed centroid latitude as a direct covariate substantially attenuates the irrigation coefficient ($\beta = +0.109$, $\rho = 0.327$; Supplementary Table S-14), confirming that the full-sample association is partially confounded with the latitudinal aridity gradient (Section 4.5). The within-Csb OLS restriction ($\beta = +0.317$, $\rho = 0.016$) provides the strongest available latitude control and retains a positive irrigation association, but the SEM estimate within Csb is marginal ($\beta = +0.264$, $\rho = 0.053$). Taken together, the evidence is consistent with demand-hardening dynamics (Grafton et al., 2018; Ward and Pulido-Velázquez, 2008), structural commitment to snowmelt-coupled irrigation amplifies drought exposure, but the irrigation coefficient cannot be claimed as fully latitude-independent with the available data.

The annual-crops association is also negatively associated with drought sensitivity and is robust to latitude control: it strengthens when latitude is added to the full-sample SEM ($\beta = -0.485$, $\rho < 0.001$) and is

confirmed within Csb (SEM $\beta = -0.565$, $\rho = 0.001$). However, the temporal pattern of this association raises a reverse-causality concern that is as important as the spatial confound affecting the irrigation finding. The annual-crop association is non-significant in the pre-drought 2007 census (SEM $\beta = -0.136$, 95% CI [−0.414, +0.142], $\rho = 0.338$) and significant in the 2021 data ($\beta = -0.322$, 95% CI [−0.543, −0.101]). However, the confidence intervals overlap substantially in the range [−0.414, −0.101], and inferring a structural change from the difference in significance between two separate models is a statistical fallacy: the 2007 non-significance may simply reflect lower statistical power rather than a true absent effect. A formal test of the coefficient difference, for example via a pooled model with a census-year interaction term, has not been conducted and would be required to claim temporal emergence. The temporal comparison therefore cannot support the inference that this association changed over time.

Independently of the temporal comparison, the sign of the 2021 coefficient raises a reverse-causality concern. The coefficient is negative, higher drought sensitivity is associated with fewer annual crops in 2021, not more. Reverse causality consistent with this sign would require that drought-sensitive watersheds reduced annual crop cultivation during the megadrought, for example, by abandoning or fallowing annual fields when water supplies were insufficient, while maintaining established perennial plantings that cannot easily be abandoned. The directionally opposite interpretation, that drought-sensitive watersheds increased annual-crop shares, would produce a positive coefficient and is ruled out by the data. Whether the negative association reflects structural buffering (annual-crop dominated systems are inherently more drought-resilient) or drought-driven abandonment of annual fields in sensitive watersheds cannot be established from the available cross-sectional observations.

The non-significance of the perennial crop coefficient in the full-sample SEM and in the within-Csb SEM should not be interpreted as evidence that perennial cultivation plays no mechanistic role in demand hardening. In Chile's Mediterranean irrigation zone, perennial cultivation and irrigation infrastructure prevalence are strongly spatially co-linear. Irrigation enables the establishment of perennial orchards and vineyards, which then lock in the water demand that creates rigidity (Grafton et al., 2018). The strong collinearity between *pct_irrigated* and *pct_perennials* (confirmed in the correlation diagnostics), combined with the spatial error term absorbing latitudinal variation shared by both predictors, means the regression cannot statistically isolate a perennial-specific effect. The more likely interpretation is that the irrigation coefficient captures a composite of supply-side coupling and the crop-type rigidity that irrigation enables, rather than infrastructure effects independent of crop type. Established demand hardening theory (Grafton et al., 2018) emphasizes

precisely the joint mechanism. Irrigation infrastructure enables inflexible perennial cultivation, and that cultivation creates the inelastic demand. The data are consistent with this joint mechanism but cannot discriminate between its components. Agricultural land-use composition is associated with WUE drought sensitivity through two patterns, each constrained by a distinct confound. The annual-crop association is robust to latitude but the causal direction is ambiguous (the negative sign is consistent with both structural buffering and drought-driven reduction of annual cultivation, and no formal test of temporal change has been conducted), while the irrigation association is constrained by spatial latitude confounding. Both should be treated as hypotheses consistent with the data rather than established causal mechanisms (Boser et al., 2024; FAO y ONU Agua, 2025; Hellegers and Van Halsema, 2021; Wang et al., 2024).

4.4. Spatial structure, global implications, and limits of adaptation

WUE coldspots are concentrated in the Aconcagua, Maipo, Rapel, Mataquito, and Maule basins (32-36°S), precisely the zone concentrating Chile's export fruit and wine production. Because the central agricultural corridor stresses simultaneously, water-market transfers under Chile's privatized Water Code have limited scope to buffer basin-scale shortfalls (Budds, 2020; Malagueño and D'Odorico, 2024; Rivera et al., 2016). Drought-driven WUE decline means more water is consumed per unit of biomass produced; sustaining production in high-sensitivity basins requires proportionally greater withdrawals precisely when supply is lowest.

The supply-failure mechanism applies wherever irrigated agriculture depends on snowmelt-fed rivers in semi-arid and Mediterranean climate zones, including California's Central Valley (Barnett et al., 2008), Spain's Ebro basin, and snowmelt-dependent networks in Iran and northern China (Immerzeel et al., 2020; Lutz et al., 2014). Institutional buffering capacity differs substantially across regions. State-managed systems with groundwater banking and drought contingency powers may partially decouple farm-gate delivery from meteorological drought signals; Chile's privatized water market, where simultaneous basin-scale droughts exhaust reallocation capacity, represents one end of a governance spectrum. Transferring Chilean quantitative findings to other regions therefore requires assessment of both hydrological coupling and institutional buffering capacity.

Where irrigation supply is hydrologically coupled to the same climate signals that drive drought, expanding irrigation infrastructure without securing supply independence may increase aggregate drought exposure. This does not argue against irrigation per se, but distinguishes between systems with independent supply and those coupled to snowmelt and precipitation, a distinction with direct relevance for investment prioritization

and drought-contingency planning (FAO y ONU Agua, 2025).

These findings have direct management implications. Water managers and planners in snowmelt-dependent irrigation systems should: (i) audit whether irrigation water rights are hydrologically coupled to the same drought signals that reduce crop productivity, since uncoupled supply (groundwater banks, interbasin transfers, reservoir buffering) is the key structural difference between drought-resilient and drought-amplifying systems; (ii) prioritize drought-contingency investment in sub-watersheds with high census-reported irrigation infrastructure prevalence and limited groundwater independence, as these show the greatest WUE sensitivity and, hypothetically, the least capacity to adjust cultivation intensity in supply-failure years; and (iii) interpret aggregate WUE gains in irrigated zones during drought periods with caution, since these may coincide with elevated drought coupling rather than genuine efficiency improvement.

4.5. Methodological limitations and future directions

All findings are associative, derived from cross-sectional observational data. The paired-census quasi-experimental design provides evidence against drought-driven adaptive confounding but cannot establish that irrigation infrastructure causally drives amplified WUE sensitivity. Findings should be interpreted as structurally stable associations consistent with the proposed mechanisms.

Key limitations are: (i) the static agricultural mask may integrate natural vegetation patches, though matorral contamination was non-significant as a control covariate ($\beta = 0.098$, $\rho = 0.509$; Supplementary Figure S-3) and a barren-exclusion dynamic filter produced virtually identical results (Supplementary Table S-7); (ii) the strong latitudinal gradient is the primary limitation for the irrigation result: aridity, crop composition, irrigation prevalence, and WUE sensitivity all co-vary with latitude in Chile (all five latitude-block holdout R^2 values are negative; Supplementary Figure S-4). Adding sub-watershed centroid latitude directly to the full-sample SEM attenuates the irrigation coefficient from $\beta = +0.422$ to $\beta = +0.109$ ($\rho = 0.327$; ΔAIC $= 20.4$), while latitude itself is highly significant ($\beta = +0.062$, $\rho < 0.001$; Supplementary Table S-14). The irrigation effect cannot be claimed as latitude-independent. The annual-crops buffering association strengthens under latitude control ($\beta = -0.485$, $\rho < 0.001$) and within Csb (SEM $\beta = -0.565$, $\rho = 0.001$), establishing it as the more robustly latitude-independent result; (iii) the census variable *pct_irrigated* does not distinguish surface water from groundwater irrigation, though the DGA streamflow validation, aquifer co-decline evidence (Donoso, 2018), and temporal coefficient stability across census years collectively suggest groundwater confounding is unlikely to explain the observed pattern; (iv) the strong spatial collinearity between irrigation infrastructure prevalence and perennial crop share in Chile's Mediterranean zone means

the regression cannot statistically isolate a perennial-specific demand-hardening effect from the irrigation coefficient; the non-significance of the perennial predictor in the SEM likely reflects a Type II error from this collinearity rather than mechanical absence of a perennial rigidity pathway; (v) the primary CASEarth WUE dataset does not distribute its internal NPP (EF-LUE) and ET (ETMonitor) component layers; because independent MODIS proxies (MOD17, MOD16) do not algebraically recombine to form the CASEarth WUE, no formal component attribution is presented and the component channel analysis previously included in this manuscript has been removed; (vi) the 2007 census comparison is unreliable for all three predictors: the heavily imputed pct_irrigated predictor (66.6% imputed with a uniform ratio that distorts cross-sectional variance) causes measurement error spillover to the correlated pct_annuals and pct_perennials coefficients in the same multiple regression model, so the 2007 coefficients cannot serve as reliable evidence for or against temporal change in any predictor; (vii) the paired-census design cannot resolve gradual within-period compositional change; longitudinal census data would allow analysis of incremental adaptation responses and the census-based framework provides a replicable template for future work (Chakraborti et al., 2023; Xie et al., 2023).

5. Conclusions

Across 127 Chilean agricultural sub-watersheds (2001–2020), four principal conclusions emerge:

1. WUE decline is spatially concentrated in the central Mediterranean zone, co-located with NPP suppression. Negative Mann-Kendall trends and FDR-significant structural breaks both concentrate in the 30°S-35°S band, identifying the sub-watersheds most tightly coupled to megadrought forcing.
2. SPEI and SPI carry practically equivalent cross-sectional information about WUE drought sensitivity. TOST equivalence within ± 0.05 R^2 margin: $\rho < 0.001$, 90% CI $[-0.004, +0.003]$. Precipitation dominates the spatial gradient in WUE sensitivity at multi-year accumulation scales.
3. Crop-composition associations with WUE drought sensitivity are observed but not causally established, each constrained by a distinct confound. Irrigation infrastructure prevalence is positively associated with drought sensitivity (SEM $\beta = +0.422$, $\rho < 0.001$) but attenuates when latitude is controlled ($\beta = +0.109$, $\rho = 0.327$), indicating partial spatial confounding consistent with a demand-hardening hypothesis. Annual-crop prevalence is negatively associated across all latitude specifications (SEM $\beta = -0.322$ to -0.565). The negative sign means drought-sensitive watersheds have fewer annuals in 2021, consistent with either structural buffering or drought-driven reduction of annual cultivation; the 2007

and 2021 confidence intervals overlap substantially and a formal test of temporal change has not been conducted, so no inference of emergence can be made from the significance comparison alone.

4. Independent snowmelt co-variation evidence is consistent with the irrigation-coupling hypothesis. Cross-product ρ(CHIRPS SPEI-12, ERA5-Land SWEI) = 0.549 in the most-irrigated quartile; ρ(CHIRPS SPEI-12, DGA streamflow) = 0.72-0.83 across five key irrigation basins; ρ(streamflow, WUE) = 0.38-0.68 in the three northern basins.

Both crop-composition patterns are hypotheses warranting longitudinal validation: the irrigation finding requires finer latitude controls and water-source disaggregation; the annual-crop finding requires direct measurement of planted-area changes across the megadrought. Neither can be treated as a definitively established causal mechanism with the available observational data. Effective drought governance in snowmelt-dependent irrigated systems requires explicit accounting for whether irrigation supply is genuinely decoupled from meteorological drought signals.

6. Funding

The National Research and Development Agency of Chile (ANID) funded this study through the drought emergency project FSEQ210022, Fondecyt Iniciación N°11190360, and Fondecyt Iniciación N°11230334. We declare that the authors have no competing interests, or other interests that might be perceived to influence the results and/or discussion reported in this paper.

7. Acknowledgements

The authors acknowledge the use of the CASEarth global cropland WUE dataset (Jiang et al., 2025), MODIS Terra products (MOD17A3HGF, MOD16A2GF) distributed by NASA Earthdata, CHIRPS v2.0 precipitation data and CHIRTS-daily temperature data provided by the Climate Hazards Center (University of California, Santa Barbara), and ERA5-Land reanalysis data provided by the European Centre for Medium-Range Weather Forecasts (ECMWF) via the Copernicus Climate Change Service (used for SWEI derivation). Agricultural census microdata were obtained from the Chilean Instituto Nacional de Estadísticas (INE). The authors declare no conflicts of interest.

8. Code and Data Availability

All analysis code is publicly available at https://github.com/frzambra/WUE_article (R scripts for all preprocessing, statistical analysis, and figure generation steps, with package versions managed via `renv` for reproducibility), enabling immediate reviewer access during manuscript evaluation. A permanent citable archive with a DOI will be deposited at Zenodo upon acceptance.

Annual cropland WUE rasters (NPP/ET, 1 km, 2001-2020) were obtained from Jiang et al. (2025), available at the CASEarth Data Platform (https://data.casearth.cn/dataset/640f0132819aec3f2b52a4bb). NPP data (zNPP) were obtained from MOD17A3HGF (MODIS Terra, 500 m, Collection 6.1) for descriptive trend comparison only. ET anomaly data (SETI-12 December) were derived from MOD16A2GF (MODIS Terra, 500 m 8-day, Collection 6.1) for descriptive trend analysis only; the formal component sensitivity decomposition analysis previously using these products has been removed as it does not algebraically reproduce the CASEarth WUE. For cross-product validation purposes, annual ET (zET) was additionally obtained from MOD16A3GF (MODIS Terra, 500 m annual, Collection 6.1; Supplementary Figure S-7). All MODIS products are available from NASA Earthdata (https://earthdata.nasa.gov). Drought index raster time series (SPEI, SPI, EDDI) were computed from CHIRPS v2.0 monthly precipitation (Funk et al., 2015) and CHIRTS-daily temperature (Funk et al., 2019), with SPEI and EDDI using FAO-56 Penman-Monteith reference evapotranspiration derived from CHIRTS. Snow Water Equivalent Index (SWEI) was derived from ERA5-Land monthly snow water equivalent reanalysis data. Agricultural census microdata for the 2007 and 2020-2021 censuses are publicly available from the Chilean Instituto Nacional de Estadísticas (INE; https://www.ine.gob.cl). Full software version details are listed in Section 2.6.

Declaration of generative AI and AI-assisted technologies in the manuscript preparation process

During the preparation of this work, the authors used Claude (Anthropic) to assist with the statistical analysis and to improve the English grammar. After using this tool, the authors reviewed and edited the content as needed and took full responsibility for the published article.

References

AghaKouchak, A., Farahmand, A., Melton, F.S., Teixeira, J., Anderson, M.C., Wardlow, B.D., Hain, C.R., 2015. Remote sensing of drought: Progress, challenges and opportunities. Reviews of Geophysics 53, 452–480. doi:10.1002/2014RG000456.

582 Barnett, T.P., Pierce, D.W., Hidalgo, H.G., Bonfils, C., Santer, B.D., Das, T., Bala, G., Wood, A.W.,
583 Nozawa, T., Mirin, A.A., et al., 2008. Human-induced changes in the hydrology of the western United
584 States. Science 319, 1080–1083. doi:10.1126/science.1152538.

585 Bivand, R., Millo, G., Piras, G., 2021. A Review of Software for Spatial Econometrics in R. Mathematics 9,
586 1276. URL: https://www.mdpi.com/2227-7390/9/11/1276, doi:10.3390/math9111276.

587 Bivand, R., Wong, D.W.S., 2018. Comparing implementations of global and local indicators of spatial
588 association. TEST 27, 716–748. doi:10.1007/s11749-018-0599-x.

589 Boisier, J., Alvarez-Garreton, C., Cordero, R., Damiani, A., Gallardo, L., Garreaud, R., Lambert, F., Ramallo,
590 C., Rojas, M., Rondanelli, R., 2018. Anthropogenic drying in central-southern chile evidenced by long-term
591 observations and climate model simulations. Elementa 6, 74. doi:10.1525/elementa.328.

592 Boser, A., Caylor, K., Larsen, A., Pascolini-Campbell, M., Reager, J., Carleton, T., 2024. Field-scale crop wa-
593 ter consumption estimates reveal potential water savings in california agriculture. Nature Communications
594 15, 2366. doi:10.1038/s41467-024-46031-2.

595 Budds, J., 2020. Securing the market: Water security and the internal contradictions of chile's water code.
596 Geoforum 113, 165–175. doi:10.1016/j.geoforum.2018.09.027.

597 Chakraborti, R., Davis, K.F., DeFries, R., Rao, N.D., Joseph, J., Ghosh, S., 2023. Crop switching for water
598 sustainability in india's food bowl yields co-benefits for food security and farmers' profits. Nature Water 1,
599 864–878. doi:10.1038/s44221-023-00135-z.

600 Croissant, Y., Millo, G., 2008. Panel data econometrics in R: The plm package. Journal of Statistical
601 Software 27, 1–43. doi:10.18637/jss.v027.i02.

602 Davis, K., Rulli, M., Seveso, A., D'Odorico, P., 2017. Increased food production and reduced water use
603 through optimized crop distribution. Nature Geoscience 10, 919–924. doi:10.1038/s41561-017-0004-5.

604 Donoso, G. (Ed.), 2018. Water Policy in Chile. Springer International Publishing, Cham. doi:10.1007/978-
605 3-319-76702-4. global Issues in Water Policy, Vol. 21.

606 Driscoll, J.C., Kraay, A.C., 1998. Consistent covariance matrix estimation with spatially dependent panel
607 data. Review of Economics and Statistics 80, 549–560. doi:10.1162/003465398557825.

608 FAO y ONU Agua, 2025. Progreso del cambio en la eficiencia del uso del agua. doi:10.4060/cd2023es.

Fox, J., Weisberg, S., 2019. An R Companion to Applied Regression. 3 ed., Sage, Thousand Oaks, CA.

Funk, C., Peterson, P., Landsfeld, M., Pedreros, D., Verdin, J., Shukla, S., Husak, G., Rowland, J., Harrison, L., Hoell, A., et al., 2015. The climate hazards infrared precipitation with stations—a new environmental record for monitoring extremes. Scientific Data 2, 1–21. doi:10.1038/sdata.2015.66.

Funk, C., Peterson, P., Peterson, S., Shukla, S., Davenport, F., Michaelsen, J., Knapp, K.R., Landsfeld, M., Husak, G., Harrison, L., et al., 2019. A high-resolution 1983–2016 t_{max} climate data record based on infrared temperatures and stations by the climate hazard center. Journal of Climate 32, 5639–5658. doi:10.1175/JCLI-D-18-0698.1.

Garreaud, R., Alvarez-Garreton, C., Barichivich, J., Boisier, J., Christie, D., Galleguillos, M., LeQuesne, C., McPhee, J., Zambrano-Bigiarini, M., 2017. The 2010-2015 mega drought in central chile: Impacts on regional hydroclimate and vegetation. Hydrology and Earth System Sciences Discussions 2017, 1–37. doi:10.5194/hess-2017-191.

Garreaud, R., Boisier, J., Rondanelli, R., Montecinos, A., Sepúlveda, H., Veloso-Aguila, D., 2020. The central chile mega drought (2010–2018): A climate dynamics perspective. International Journal of Climatology 40, 421–439. doi:10.1002/joc.6219.

Gebrechorkos, S.H., Sheffield, J., Vicente-Serrano, S.M., Funk, C., Miralles, D.G., Peng, J., Dyer, E., Talib, J., Beck, H.E., Singer, M.B., Dadson, S.J., 2025. Warming accelerates global drought severity. Nature doi:10.1038/s41586-025-09047-2.

Grafton, R.Q., Williams, J., Perry, C.J., Molle, F., Ringler, C., Steduto, P., Udall, B., Wheeler, S.A., Wang, Y., Garrick, D., et al., 2018. The paradox of irrigation efficiency. Science 361, 748–750. doi:10.1126/science.aat9314.

Hellegers, P., Van Halsema, G., 2021. Sdg indicator 6.4.1 “change in water use efficiency over time”: Methodological flaws and suggestions for improvement. Science of The Total Environment 801, 149431. doi:10.1016/j.scitotenv.2021.149431.

Hijmans, R.J., 2025. terra: Spatial Data Analysis. URL: https://CRAN.R-project.org/package=terra, doi:10.32614/CRAN.package.terra. r package version 1.8-54.

Hobbins, M.T., Wood, A., McEvoy, D.J., Huntington, J.L., Morton, C., Anderson, M., Hain, C., 2016. The

evaporative demand drought index. part i: Linking drought evolution to variations in evaporative demand. Journal of Hydrometeorology 17, 1745–1761. doi:10.1175/JHM-D-15-0121.1.

Hoekstra, A., Mekonnen, M., 2012. The water footprint of humanity. Proceedings of the National Academy of Sciences 109, 3232–3237. doi:10.1073/pnas.1109936109.

Hoover, D., Abendroth, L., Browning, D., Saha, A., Snyder, K., Wagle, P., Witthaus, L., Baffaut, C., Biederman, J., Bosch, D., Bracho, R., Busch, D., Clark, P., Ellsworth, P., Fay, P., Flerchinger, G., Kearney, S., Levers, L., Saliendra, N., Schmer, M., Schomberg, H., Scott, R., 2023. Indicators of water use efficiency across diverse agroecosystems and spatiotemporal scales. Science of The Total Environment 864, 160992. doi:10.1016/j.scitotenv.2022.160992.

Howden, S., Soussana, J.F., Tubiello, F., Chhetri, N., Dunlop, M., Meinke, H., 2007. Adapting agriculture to climate change. Proceedings of the National Academy of Sciences 104, 19691–19696. doi:10.1073/pnas.0701890104.

Hu, G., Jia, L., 2015. Monitoring of Evapotranspiration in a Semi-Arid Inland River Basin by Combining Microwave and Optical Remote Sensing Observations. Remote Sensing 7, 3056–3087. URL: https://www.mdpi.com/2072-4292/7/3/3056, doi:10.3390/rs70303056.

Immerzeel, W.W., Lutz, A.F., Andrade, M., Bahl, A., Biemans, H., Bolch, T., Hyde, S., Brumby, S., Davies, B.J., Elmore, A.C., et al., 2020. Importance and vulnerability of the world's water towers. Nature 577, 364–369. doi:10.1038/s41586-019-1822-y.

INE, 2007. VII Censo nacional agropecuario y forestal. Instituto Nacional de Estadística. Informe Agropecuarias 2007. Technical Report.

INE, 2021. VIII Censo Nacional Agropecuario y Forestal. Instituto Nacional de Estadísticas. Santiago, Chile. URL: https://www.ine.gob.cl/estadisticas-por-tema/agricultura-y-medio-ambiente/censo-agropecuario. resultados finales publicados en octubre de 2022.

Ito, A., Inatomi, M., 2012. Water-use efficiency of the terrestrial biosphere: A model analysis focusing on interactions between the global carbon and water cycles. Journal of Hydrometeorology 13, 681–694. doi:10.1175/JHM-D-10-05034.1.

Jiang, M., Zheng, C., Jia, L., Chen, J., 2025. A 20-year dataset (2001–2020) of global cropland water-use efficiency at 1-km grid resolution. Scientific Data 12, 574. doi:10.1038/s41597-025-04904-1.

Li, F., Xiao, J., Chen, J., Ballantyne, A., Jin, K., Li, B., Abraha, M., John, R., 2023. Global water use efficiency saturation due to increased vapor pressure deficit. Science 381, 672–677. doi:10.1126/science.adf5041.

Lutz, A.F., Immerzeel, W.W., Shrestha, A.B., Bierkens, M.F., 2014. Consistent increase in High Asia's runoff due to increasing glacier melt and precipitation. Nature Climate Change 4, 587–592. doi:10.1038/nclimate2237.

Malagueño, B.R., D'Odorico, P., 2024. ¿libre de la maleza estatista? Assessing neoliberal promises and water markets in Chile. Earth's Future doi:10.1029/2024EF004963.

McEvoy, D.J., Huntington, J.L., Hobbins, M.T., Wood, A., Morton, C., Anderson, M., Hain, C., 2016. The evaporative demand drought index. part ii: Conus-wide assessment against common drought indicators. Journal of Hydrometeorology 17, 1763–1779. doi:10.1175/JHM-D-15-0122.1.

Mckee, T.B., Doesken, N.J., Kleist, J., 1993. The relationship of drought frequency and duration to time scales, in: Proceedings of the Ninth Conference on Applied Climatology, American Metereological Society, Boston. pp. 179–184.

Patakamuri, S.K., O'Brien, N., 2021. modifiedmk: Modified Versions of Mann Kendall and Spearman's Rho Trend Tests. URL: https://CRAN.R-project.org/package=modifiedmk, doi:10.32614/CRAN.package.modifiedmk. r package version 1.6.

Pebesma, E., 2018. Simple Features for R: Standardized Support for Spatial Vector Data. The R Journal 10, 439–446. URL: https://doi.org/10.32614/RJ-2018-009, doi:10.32614/RJ-2018-009.

Pebesma, E., Bivand, R., 2023. Spatial Data Science: With applications in R. Chapman and Hall/CRC. URL: https://r-spatial.org/book/, doi:10.1201/9780429459016.

Pedersen, T.L., 2025. patchwork: The Composer of Plots. URL: https://CRAN.R-project.org/package=patchwork, doi:10.32614/CRAN.package.patchwork. r package version 1.3.1.

Pettitt, A.N., 1979. A non-parametric approach to the change-point problem. Journal of the Royal Statistical Society: Series C (Applied Statistics) 28, 126–135. doi:10.2307/2346729.

Pohlert, T., 2023. trend: Non-Parametric Trend Tests and Change-Point Detection. URL: https://CRAN.R-project.org/package=trend, doi:10.32614/CRAN.package.trend. r package version 1.1.6.

R Core Team, 2025. R: A Language and Environment for Statistical Computing. R Foundation for Statistical Computing. Vienna, Austria. URL: https://www.R-project.org/.

692 Rivera, D., Godoy-Faúndez, A., Lillo, M., Alvez, A., Delgado, V., Gonzalo-Martín, C., Menasalvas, E.,
693 Costumero, R., García-Pedrero, Á., 2016. Legal disputes as a proxy for regional conflicts over water rights
694 in chile. Journal of Hydrology 535, 36–45. doi:10.1016/j.jhydrol.2016.01.057.

695 Running, S., Mu, Q., Zhao, M., Moreno, A., 2021. MODIS/Terra net evapotranspiration Gap-Filled 8-day
696 L4 global 500m SIN grid V061.

697 Tennekes, M., 2018. tmap: Thematic maps in R. Journal of Statistical Software 84, 1–39. doi:10.18637/
698 jss.v084.i06.

699 Vicente-Serrano, S.M., Beguería, S., López-Moreno, J.I., 2010. A multiscalar drought index sensitive to global
700 warming: The standardized precipitation evapotranspiration index. Journal of Climate 23, 1696–1718.
701 doi:10.1175/2009JCLI2909.1.

702 Wallace, J., 2000. Increasing agricultural water use efficiency to meet future food production. Agriculture,
703 Ecosystems & Environment 82, 105–119. URL: http://dx.doi.org/10.1016/S0167-8809(00)00220-6, doi:10.
704 1016/s0167-8809(00)00220-6.

705 Wang, T., Sun, S., Yin, Y., Zhao, J., Tang, Y., Wang, Y., Gao, F., Luan, X., 2024. Status of crop
706 water use efficiency evaluation methods: A review. Agricultural and Forest Meteorology 349, 109961.
707 doi:10.1016/j.agrformet.2024.109961.

708 Ward, F.A., Pulido-Velázquez, M., 2008. Water conservation in irrigation can increase water use. Proceedings
709 of the National Academy of Sciences 105, 18215–18220. doi:10.1073/pnas.0805554105.

710 Wickham, H., 2016. ggplot2: Elegant Graphics for Data Analysis. Springer-Verlag New York. URL:
711 https://ggplot2.tidyverse.org.

712 Wickham, H., Averick, M., Bryan, J., Chang, W., McGowan, L.D., François, R., Grolemund, G., Hayes, A.,
713 Henry, L., Hester, J., Kuhn, M., Pedersen, T.L., Miller, E., Bache, S.M., Müller, K., Ooms, J., Robinson,
714 D., Seidel, D.P., Spinu, V., Takahashi, K., Vaughan, D., Wilke, C., Woo, K., Yutani, H., 2019. Welcome
715 to the tidyverse. Journal of Open Source Software 4, 1686. doi:10.21105/joss.01686.

716 Xie, W., Zhu, A., Ali, T., Zhang, Z., Chen, X., Wu, F., Huang, J., Davis, K., 2023. Crop switching can enhance
717 environmental sustainability and farmer incomes in china. Nature 616, 300–305. doi:10.1038/s41586-
718 023-05799-x.

719 Yu, L., Gao, X., Zhao, X., 2020. Global synthesis of the impact of droughts on crops' water-use efficiency
720 (WUE): Towards both high WUE and productivity. Agricultural Systems 177, 102723. URL: https:
721 //linkinghub.elsevier.com/retrieve/pii/S0308521X19301568, doi:10.1016/j.agsy.2019.102723.

722 Zambrano, F., Vrieling, A., Meza, F., Duran-Llacer, I., Fernández, F., Venegas-González, A., Raab, N.,
723 Craven, D., 2025. From Drought to Aridification: Land-Cover Fingerprints of a Drying Chile. Earth's
724 Future 13, e2025EF006744. URL: https://agupubs.onlinelibrary.wiley.com/doi/10.1029/2025EF006744,
725 doi:10.1029/2025EF006744.